Stochastic Neurography

S. Jaume[1], M. Loepprich[2], E.J. Schmidt[2], R. Kikinis[2]

1 - MIT Computer Science and Artificial Intelligence Laboratory

2 - Brigham and Women's Hospital, Harvard Medical School

Contact: Sylvain Jaume, PhD - sylvain@csail.mit.edu

Introduction

Neurography is the imaging of the nerves in a volumetric scan, e.g. CT or MRI, to create a neuroanatomical map specific to the subject and understand which part of the body each nerve controls. Visualizing the network of nerves and understanding their functions is particularly important prior to and during surgery when the neurosurgeon needs to access a region of interest and to avoid to damage a nerve, which could lead to a limb paralysis. Although neurography has received a large interest for mapping the nerves and their functions, the creation and visualization of the nerve map is still time-consuming and thus seldom performed in either clinical or research applications.

We propose to automate this task using a statistical method for the detection of the nerve orientations and a stochastic process to integrate the nerve tracts over the orientation vector field. This fully automated tracking method is the first attempt to visualize and understand the neuroanatomy of the subject.

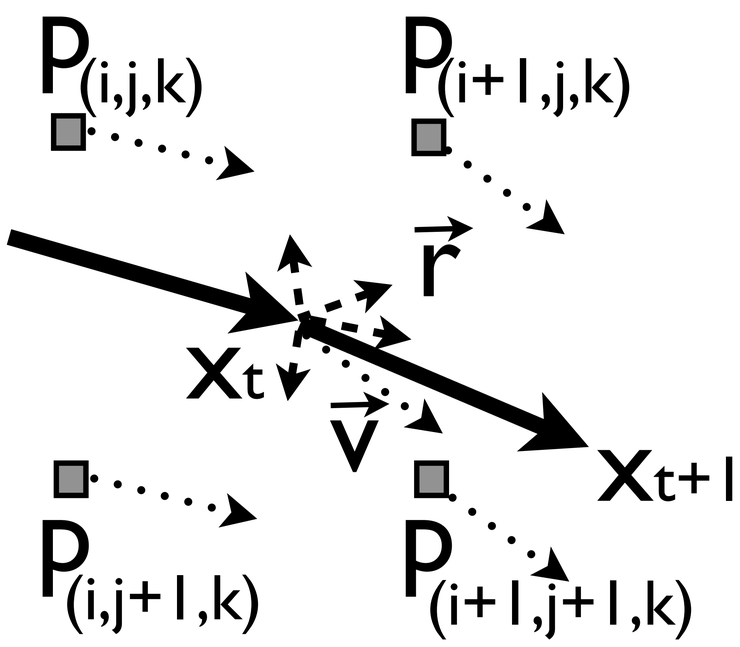

Figure 1. The position of the seeds evolves in a stochastic fashion as they propagate through the MRI volume.

Method

We first create a dense vector field V within the volumetric image. At each position x we define v = V(x) as the axis of a local cylindrical model fitting the image. This model represents a small section of a nerve as a pair of co-axial cylinders with equal length. The two cylinders define two volumetric region: first the region R_{in} inside the inner cylinder and second the region R_{out} between the inner and outer cylinders.

The fitting of the model is achieved by exploring a number of orientations and computing the distributions of intensities in R_{in} and in R_{out}. Let's call these statistical distributions H_{in} and H_{out}. The orientation for the fitting model is the orientation that maximizes the distance between H_{in} and H_{out}. Our distance metric is defined as:

$$\| H_{in}, H_{out} \| = - \Sigma(H_{in} \cap H_{out}) / \Sigma(H_{in} + H_{out})$$

where Σ counts the number of samples in a distribution subset. When H_{in} and H_{out} covers different areas in the intensity spectrum the statistical distance is maximized. The optimal orientation π at the position x is:

$$\pi(x) = \text{argmax}(\| H_{in}(x,\omega), H_{out}(x,\omega) \|) \text{ with } \omega \in \Omega$$

where ω is the orientation of the fitting model, Ω is the space of orientations that we explore, H_{in} is the intensity distribution inside the inner cylinder, H_{out} is the intensity distribution between the inner cylinder and the outer cylinder.

Second we integrate the vector field using a stochastic process to track the nerves starting from a set of seed points. The seed points are automatically generated according to a random sampling process. Starting from a position x_t at time t=0 the following position is computed based on this equation:

$$x_{t+1} = x_t + V(x_t) + \lambda.r$$

where $V(x_t)$ is the vector interpolated within the vector field, r is a random unit vector and λ is a scaling factor.

We generate a number of random vectors r and define a set of positions x_{t+1}. We then retain the position x_{t+1} which maximizes the distance metric computed above.

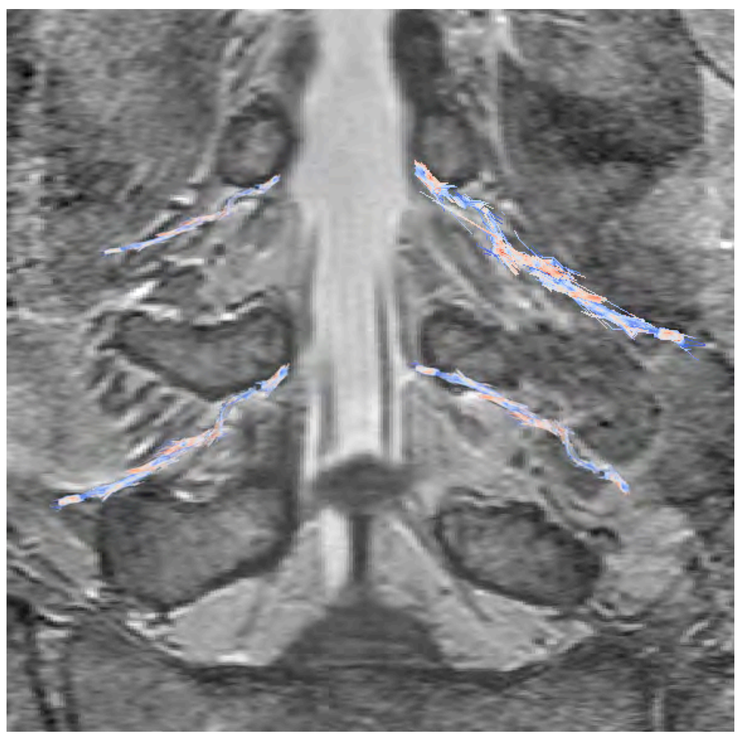

Figure 2. Segmented nerve tracts (blue-red) as they exit the lumbar spine. Viewing the nerves intra-operatively helps minimally-invasive surgery for disk herniation removal.

Results

We applied our algorithm to MRI images of the lower spine. We created the map of the nerve bundles exiting the spinal cord between the L3, L4 and L5 vertebrae. Figure 1 illustrates the stochastic process that we applied to create the nerve tract. The tract moves from position x_t to x_{t+1} with the addition of a random vector r and a vector v interpolated in the image-dependent vector field.

Figure 2 shows our results overlaid on one slice of the MRI volume. The brightest area that spans the image vertically is the cerebrospinal fluid (CSF). The spinal nerves (vertical dark lines) are visible in the center. The results of our stochastic neurography are indicates by two bundles on each side of the spine. The bundles are colored from blue to red based on local curvature to be visible on the gray scale MRI image.

Figure 3 is a close-up on the right bundle shows the nerve tracts as they exits the spinal cord. The figure indicates the effect of the random vector that allows to locally explore different image positions and to improve the finding of the nerve path.

Figure 4 shows a 3D rendering of the L3 vertebra and one nerve bundle exiting the spinal cord through the lateral foramen. The images in this figure show the nerve tracts from a view similar to coronal, sagittal and axial slices. The lower right image is a 3D view from a oblique view point to highlight the volumetric structure of the vertebra and the nerve bundle.

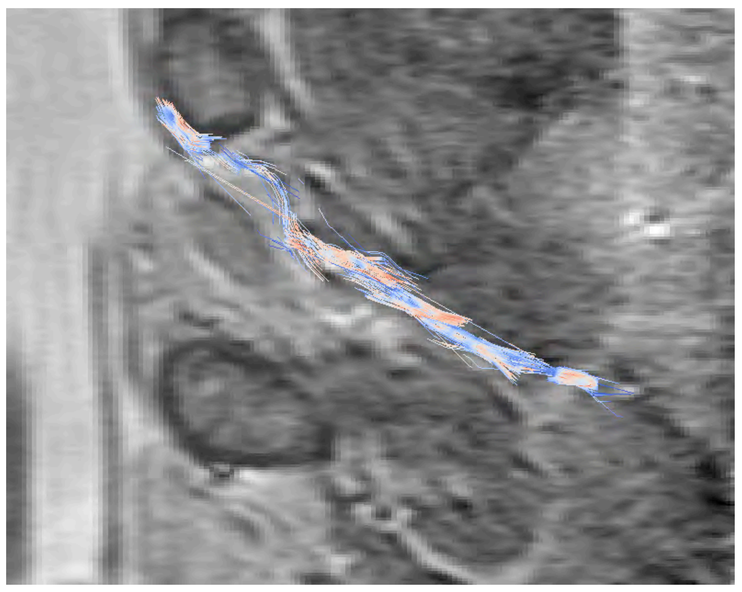

Figure 3. Close-up showing one nerve bundle overlaid on an MRI slice. Our results successfully follow the nerve bundle.

Conclusion

We have presented the first method for automatically creating a map of the nerves in volumetric MRI data. Our method is based on a stochastic process to generate a set of paths that model the nerve bundles connecting the brain and the functions of the body. First a vector field is computed from the intensity values of the MRI data. Then a number of random vectors are generated at every time step to create a path within the volumetric vector field. The created segments can be visualized on the MRI slices to indicate the connections of the nerve bundles.

We have tested our method on spine MRI images and created an anatomical map that follows the nerve bundles exiting the spinal cord. The overlay of our results on the MRI slices indicates that stochastic neurography can successfully provide a subject-specific map of the nerves. These promising results could save the neuroradiologist and the neuroscientist from the time-consuming and error-prone task of manually tracking nerves across MRI slices.

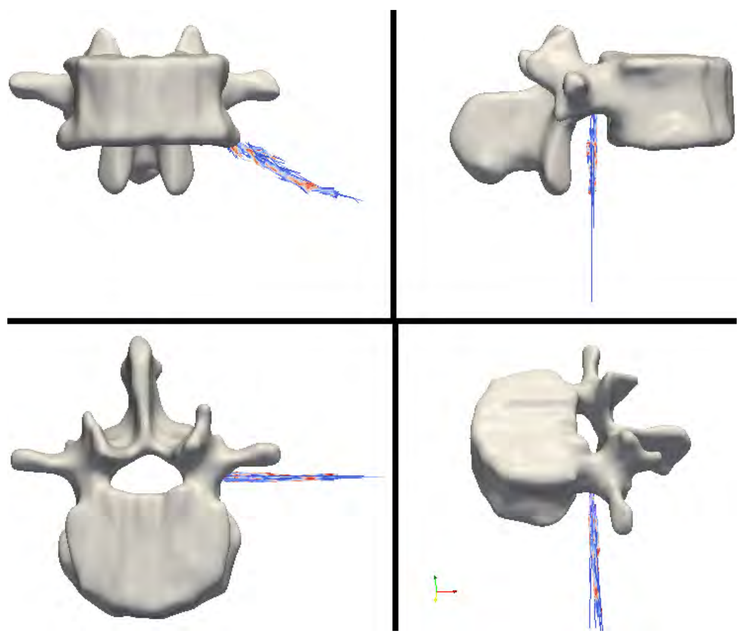

Figure 4. 3D renderings of the L3 vertebra and nerve passing through the foramen. Our 3DSlicer implementation can be applied automatically during MRI-guided surgery.

References

[1] E.J. Schmidt, A. Shankaranarayanan, S. Jaume, G. Danagoulian, S. Mukundan, K.S. Nayak, Wide-Band Steady State Free Precession with Small Diffusion Gradients for Spine Imaging: Application to Superior Nerve Visualization, ISMRM 2010.

[2] P. Basser et al., In Vivo Fiber Tractography Using DT-MRI Data, Magnetic Resonance in Medicine, 2000, vol. 44, pp. 625-632.

[3] M. Bjornemo et al., Regularized Stochastic White Matter Tractography Using Diffusion Tensor MRI, MICCAI 2002, pp 435-442

[4] T. Behrens et al., Characterization and Propagation of Uncertainty in Diffusion Weighted MR Imaging, Magnetic Resonance in Medicine, 2003, vol. 50, pp. 1077-1088.

[5] O. Friman et al., A Bayesian Approach for Stochastic White Matter Tractography, IEEE Transactions on Medical Imaging, 2006, vol. 25, no. 8, pp. 965-978.

[6] D. Jones et al., Confidence Mapping in Diffusion Tensor Magnetic Resonance Imaging Tractography Using a Bootstrap Approach, Magnetic Resonance in Medicine, 2005, vol. 5, pp. 1143-1149.

[7] A. Lazar et al., Bootstrap White Matter Tractography (boot-trac), NeuroImage, 2005, vol. 24, pp. 524-532.

[8] S. Mori et al., Three Dimensional Tracking of Axonal Projections in the Brain by Magnetic Resonance Imaging, Annals of Neurology, 1999, vol. 45, pp. 265-269.

[9] J. Berman et al., Quantitative Diffusion Tensor MRI Fiber Tractography of Sensorimotor White Matter Development in Premature Infants, NeuroImage, 2005, pp. 862-871.

[10] T.-S. Yo et al., Quantifying Brain Connectivity: A Comparative Tractography Study', MICCAI, 2009, vol. 5761, pp. 886-893.

Acknowledgment

This work is part of National Alliance for Medical Image Computing (NAMIC) funded by the NIH Grant U54 EB005149.